A computational investigation of thermodynamics, structure, dynamics and solvation behavior in modified water models

Swaroop Chatterjee,[1] Pablo G. Debenedetti,[1,a)] Frank H. Stillinger,[2] and Ruth M. Lynden-Bell[3,4]

[1]*Department of Chemical Engineering, Princeton University, Princeton, New Jersey 08544, USA*
[2]*Department of Chemistry, Princeton University, Princeton, New Jersey 08544, USA*
[3]*University Chemical Laboratory, Lensfield Road, Cambridge CB2 1EW, United Kingdom*
[4]*Atomistic Simulation Centre, School of Mathematics and Physics, Queen's University, Belfast BT7 1NN, United Kingdom*

We investigate the properties of geometrically modified water models by performing molecular dynamics simulations of perturbations of the extended simple point charge (SPC/E) model of water over a wide range of temperatures at 1 bar. The geometric modification consists of altering the H–O–H angle in SPC/E. The dipole moment is held constant by altering the O–H bond length, while the electrostatic charges are left unchanged. We find that a H–O–H angle of at least 100° is necessary for the appearance of density anomalies and of solubility extrema with respect to temperature for small apolar solutes. We observe the occurrence of two incompatible types of structural order in these models: Tetrahedral, with waterlike translational order for bent models with H–O–H angles in excess of 100°; and linear, with Lennard–Jones–like orientationally averaged translational order for smaller H–O–H angles. Increasing the H–O–H angle causes the density to increase, while at the same time shifting waterlike anomalies to progressively higher temperatures. For bent models with H–O–H angle greater than SPC/E's, we observe arrest of translational motion at 300 K (115°) and 330 K (120°). © *2008 American Institute of Physics*.
[DOI: 10.1063/1.2841127]

I. INTRODUCTION

Molecular interactions and the statistical ordering they produce under variable external conditions create the wide variations in observable properties among different substances. Liquid water's many anomalous properties,[1] in pure form and in solution, are likewise outcomes of its molecular interactions and resultant statistical ordering. Molecular simulations,[2–5] not limited by the constraints of experiments, offer an ideal route for studying the individual contributions of different aspects of water's molecular interactions to its macroscopic properties. The current study seeks to determine the effect of perturbing the molecular geometry of water on its thermodynamics, dynamics, and structural ordering, as well as on its solvation thermodynamics with respect to nonpolar solutes.

Our work adds to a number of recent studies[2–5] that address the effect of perturbations of water's molecular interactions on its bulk properties. Bergman and Lynden-Bell[2] investigated the relation between network structure and solvation properties with respect to simple charged solutes. Those authors found that when the H–O–H angle in water is reduced below 90°, the liquid adopts a one-dimensional chainlike structure instead of a three-dimensional tetrahedral network. In that study, the H–O–H angle was reduced from 109.47°, the value used in the extended simple point charge model (SPC/E),[6] to 90° and 60° ("bent models"). This caused

a dramatic change in the spatial arrangement adopted by water molecules. Two linearly arranged H-bonded neighbor clouds in the first neighbor shell around a central water molecule were observed in the oxygen-oxygen spatial distribution function[7–9] (defined in Sec. II C) for the smaller H–O–H angle case, in place of the distorted tetrahedral arrangement typically observed for SPC/E water. The change in molecular arrangement upon reducing the H–O–H angle was also accompanied by an absence of closed one-dimensional loops of hydrogen-bonded molecules that are normally present in water.

A subsequent study[3] investigated the effect of varying the relative strength of the dispersive and Coulombic contributions to water's pairwise molecular interactions ("hybrid models"). Upon reducing the strength of the electrostatic contributions, a progressive breakdown of tetrahedrality occurred, accompanied by the emergence of Lennard–Jones–like structural order. Interestingly, the authors noted that this evolution from waterlike to Lennard–Jones–like structural order occurs in such a way that there is a near-total loss of structure beyond the first peak in the oxygen-oxygen pair correlation function $g(r)$ at intermediate values of the relative strength of electrostatic interactions. As we show in Sec. III, we find an analogous evolution of structural order upon altering the geometry of the water molecule.

Yet another study[4] focused on the combined effect of changing the relative strength of electrostatic and dispersive forces, and of water molecule geometry, on solvation of apolar solutes at 1 bar and 298 K. Two types of modifications of

---

a)Electronic mail: pdebene@princeton.edu.
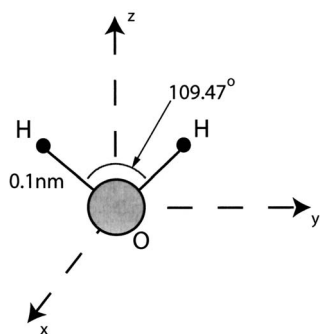
128, 124511-1

FIG. 1. Schematic representation of the SPC/E model (Ref. 6) for water. The relative size of the atoms is exaggerated for visual ease. This orientation of the molecule with respect to the reference axes, where the molecule is placed in the *z*-*y* plane and the *z*-axis bisects the H–O–H angle, is used to generate the oxygen-oxygen spatial distribution function, which is introduced in Sec. II C.

the SPC/E model were investigated. The first type was geometric alteration (bent models) where the H–O–H angle in the SPC/E model was reduced to 60° and 90°, while the second type of alteration consisted of tuning the relative strength of the Coulombic and dispersive contributions to the pair potential (hybrid models), as discussed before. Those authors showed that the solubility of apolar solutes in hybrid models decreased as the liquid structure became more densely packed (Lennard–Jones–like). The structural ordering of the bent models was substantially different from that observed in both SPC/E water and the hybrid models, with an increasing tendency to form chains observed upon decreasing the H–O–H angle. In addition, the ability of the bent model to dissolve hydrophobic solutes increased upon reducing the H–O–H angle to 60°. The reason for the decreased solvophobicity was ascribed to the chainlike structure in these bent models which have lower H–O–H angles as compared to SPC/E water.

Finally, a more recent study[5] investigated the effect of altering the electrostatic strength in two commonly used water models, SPC/E and TIP3P,[10] by interchanging the atomic charges between models. Simulations of these perturbed models in the fluid phase revealed a minimal effect on the respective structures.

The aim of the current study is to examine the effect of perturbing the geometry of the water molecule on its structure, translational dynamics, equation of state, as well as on its solvation thermodynamics with respect to nonpolar solutes, over a broad range of temperatures, at ambient pressure.

Specifically, we perturb the H–O–H angle of the water molecule. Using the SPC/E model as a base case, we consider a number of bent models with H–O–H angles ranging from 60° to 120°. We therefore seek to add to the current understanding on the relationship between water's structural, dynamic, and thermodynamic properties, and the underlying intermolecular forces. The paper is structured as follows. We provide a description of the model along with simulation and analysis methods used in our study in Sec. II. Section III contains a discussion of our results. Finally, we present our conclusions in Sec. IV.

II. METHODS

A. Model

The SPC/E model[6] considers water to be a rigid molecule with three point charges located at the oxygen and the two hydrogen atomic centers. In addition, dispersive Lennard–Jones interactions are associated with the oxygen atom.[6] The geometry of the model is illustrated schematically in Fig. 1. The point charges are $-0.8476e$ and $0.4238e$ for oxygen and hydrogen, respectively. The nearly tetrahedral H–O–H angle, along with the chosen values for the O–H bond length, electrostatic charges, and Lennard–Jones parameters, favor a tetrahedral structural ordering for water molecules.

In the "bent" models, the H–O–H angle is varied between 60° and 120°. The atomic charges and Lennard–Jones parameters for each model are kept constant as in the original SPC/E model, while the O–H distance (1 Å for SPC/E) is varied so that the molecule's dipole moment μ remains unaltered at 2.35 D. The resulting O–H distances (r_{OH}) range from 0.67 Å (60°) to 1.15 Å (120°). The change in O–H distances leads to a change in strength of the model's quadrupolar interactions. A convenient measure of this strength, which is not dependent on the choice of coordinate origin, is given by[11,12]

$$Q_T = \frac{3(r_{OH} \sin \theta)^2}{4 r_{OH} \cos \theta} \mu, \tag{1}$$

where 2θ is the H–O–H angle. The value of Q_T varies from 0.34 D Å (60°) to 3.05 D Å (120°). In recent studies, Abascal and Vega[11,12] related the variation of Q_T in different water models to their melting temperature and phase behavior.

Table I compares the perturbations considered in this study to those in previously published work. In what follows,

TABLE I. Definition of various modified water models. (Refs. 2–5). DM: Dipole moment of bent molecule; AC: Atomic charges; O–H: O–H bond length; LJ: LJ contribution to intermolecular potential.

Source	Modification	Altered?			
		DM	AC	O–H	LJ
Reference 2	H–O–H angle: 60°, 90°	No	No	Yes	Yes
Reference 3	Electrostatic strength	No	No	No	Yes
Reference 4	Electrostatic strength	No	No	No	Yes
Reference 4	H–O–H angle: 60°, 90°	No	No	Yes	Yes
Reference 5	Electrostatic strength	Yes	Yes	No	No
Present Work	60° ≤ H–O–H Angle ≤120°	No	No	Yes	No

we refer to the various bent models by the value of their respective H–O–H angles, e.g., B60, B115, etc.

B. Simulation

For each model, both canonical (NVT) and isobaric-isothermal (NPT) molecular dynamics (MD) simulations were performed. A Berendsen[13] thermostat and barostat were used to regulate the temperature and pressure, with time constants of 0.1 and 0.5 ps, respectively. The Verlet algorithm[14] with a time step size of 1 fs was used to integrate the equations of motion. The intramolecular geometry was constrained by a SHAKE routine[15] with a tolerance of 10^{-8} Å. Periodic boundary conditions were employed. The Lennard–Jones (LJ) contribution to the intermolecular potential was truncated and shifted[14] beyond $2.5\sigma_w$, where σ_w is the size parameter of the SPC/E model. The standard SPC/E value for the LJ well depth $\epsilon_w = 0.6502$ kJ/mol was used. The Ewald summation method[14] was used to calculate the long-range electrostatic interactions. The real space contribution was calculated for all nearest-neighbor images. Using the parameters employed by Svishchev and Kusalik[8] as a guide, the Fourier space sum was calculated over the first 400 wave vectors with a dimensionless convergence parameter κ of 6.4.

For each model, 1000 molecules were simulated using the following protocol. The equilibrium density was obtained at different temperatures at 1 bar in the NPT ensemble. The length of these runs was typically 1 ns. The equation of state thus obtained was used to set the system density for NVT runs such that all data were obtained at 1 bar.

The solvation behavior of LJ solute molecules was also studied in this work. For this purpose, two solute sizes ($\sigma_s = 3.16$ and 6 Å) were considered. The solute's LJ well depth ϵ_s was set equal to that of SPC/E water. Solute-water interactions were calculated using standard mixing rules, $\epsilon_{sw} = \sqrt{\epsilon_s\epsilon_w}$ and $\sigma_{sw} = 1/2(\sigma_s + \sigma_w)$. The Widom particle-insertion method[16] was used to calculate the solute's excess chemical potential μ_s^{ex} at infinite dilution relative to an ideal gas at the same density and temperature,

$$\mu_s^{ex}/k_BT = -\ln(\langle\exp(-U_{sw}/k_BT)\rangle_{neat}), \tag{2}$$

where U_{sw} is the energy of interaction between a randomly inserted solute molecule and the neat liquid, T is the temperature, and k_B is Boltzmann's constant. The thermal average in Eq. (2) is over the equilibrated solvent. In our study, the averaging was conducted over 10^6 configurations with 1000 successful insertions per configuration. A distance cutoff of $2.5\sigma_{sw}$ was used in the interaction energy calculation. The excess chemical potential is thus obtained from the running average of the Boltzmann factor for the solute-neat liquid interaction over the course of an NVT simulation of the neat liquid.

In order to characterize the structural order in supercooled and glassy states, a series of NVT runs were conducted such that the neat liquid was cooled isochorically starting from its equilibrium state at 1 bar and 400 K. The system was cooled at a constant rate of 30 K/ns from 400 to 10 K. At regular intervals of 10 ps, cooling was interrupted and the system was equilibrated at constant temperature to allow the collection of configurations for structural order analysis. During these periods, 100 configurations were stored and subsequently used as starting points to determine the underlying inherent structure, i.e., the configuration corresponding to a local potential energy minimum.[17] A conjugate gradient method was employed to achieve this minimization using a tolerance of 10^{-15} kJ/mol for the energy between two successive iterations.[18] Various order metrics were subsequently computed in each inherent structure along with its precursor quenched configuration.

C. Analysis

The use of oxygen-oxygen spatial distribution functions $g(r,\Omega)$ in studying the structure of water was first introduced by Svishchev and Kusalik.[8] They argued that in systems whose particles do not have spherical symmetry, such as water, a great deal of structural information is lost by simply considering the spherically averaged radial distribution of molecules. The angular distribution contains valuable information about the relative orientation of molecules in space. The oxygen-oxygen spatial distribution function is nothing but the pair correlation function of oxygen atoms with the radial and angular orientation contributions left intact. While the full orientation-dependent correlation function of the rigid water molecule ought to include five angular degrees of freedom, the oxygen-oxygen spatial distribution function employed in our work only considers the two angular degrees of freedom associated with the position of an oxygen atom relative to another. In order to calculate this function, each molecule in the system is considered in turn. The reference frame is translated and rotated such that the molecule under consideration is in the same orientation as the SPC/E water molecule shown in Fig. 1. The coordinates of the neighboring oxygen atoms are then transformed to this reference frame using standard methods involving Euler angles and rotation matrices.[19] The local spatial frame around each molecule is decomposed into $150\times150\times150$ bins for the radial r, polar θ, and azimuthal ϕ contributions to the spatial distribution function. The number of oxygen atoms in a spatial bin $n(r,\Omega=\{\theta,\phi\})$ is then related to $g(r,\Omega)$ using the relation

$$n(r,\Omega) = \rho g(r,\Omega)r^2\sin\theta\Delta r\Delta\theta\Delta\phi, \tag{3}$$

where Δr, $\Delta\theta$, and $\Delta\phi$ are the dimensions of each bin and ρ is the density. The isosurfaces $g(r,\Omega)=$ const can be used to visualize the spatial distribution of neighbors around a central molecule.

Structural order parameters were calculated both for the quenched and inherent structure configurations. Translational and orientational order metrics have often been used in recent years to study structural order in liquids, glasses, and particle packings.[20–22] Following Errington and Debenedetti,[23] we use an orientational order parameter appropriate for systems with local tetrahedral order.[24] The translational order parameter[20,21] τ can be calculated from the radial distribution function $g(r)$,

$$\tau = \frac{1}{\xi_c} \int_0^{\xi_c} |g(\xi) - 1| d\xi, \qquad (4)$$

where $\xi = r\rho^{1/3}$ is a rescaled distance between oxygen atoms and $\xi_c = 2.5$ is a cutoff distance. The definition implies that $\tau = 0$ for an ideal gas. Correlations between molecules and atoms lead to a nonzero τ, which increases as the correlations become long ranged. This is indicative of the formation of successive local neighbor shells around molecules.

The orientational metric q is given by[23,24]

$$q = 1 - \frac{3}{8} \sum_{j=1}^{3} \sum_{k=j+1}^{4} \left(\cos \psi_{jk} + \frac{1}{3} \right)^2, \qquad (5)$$

where ψ_{jk} is the O–O–O angle formed by a central molecule and its nearest neighbors j and k (≤ 4). The range of possible values for q is between -3 and 1. Averaging this order parameter $\langle q \rangle$ for uncorrelated particles (ideal gas case), we get[23] $\langle q \rangle = 0$. In the remainder of the paper, the notation q will automatically represent $\langle q \rangle$, where averaging is done over all atoms and all configurations. In a perfect tetrahedral network, $\cos \psi_{jk} = -1/3$, which gives $q = 1$. The value of q therefore measures the degree of tetrahedrality in the system.

III. RESULTS AND DISCUSSION

A. Equation of state

All the results presented in this section were obtained at a pressure of 1 bar. As discussed in the previous section, *NPT* MD simulations were used to obtain the equation of state for the different bent water models at this pressure [see Fig. 2(a)]. The figure shows the liquid-phase equation of state in the form of density versus temperature for each model. We find that models B120, B115, and SPC/E are not diffusive for temperatures lower than 330, 300, and 220 K, respectively, and hence do not equilibrate under these conditions in the course of *NVT* simulations.

As mentioned earlier in Sec. II A, the change in bond angle is associated with an O–H distance variation across the different bent models in order to conserve the dipole moment. It leads to a modification of the quadrupole interaction strength Q_T [Eq. (1)]. According to Abascal and Vega,[11,12] the value of Q_T is positively correlated with melting temperature. Therefore, the expectation is that melting temperature of the different bent models will also follow the same trend, wherein the melting temperatures would be such that $T_{m,B60} < T_{m,B90} < \dots < T_{m,B120}$. The expected increase in the melting temperature of B115 and B120 over that of SPC/E is consistent with glass formation in these two models as the reason for the loss of diffusive behavior for temperatures lower than 330 and 300 K, respectively.

One of the most distinctive anomalies of liquid water is the density maximum and the consequent negative thermal expansion at low temperature (expansion upon isobaric cooling). The anomaly arises due to the energetically favorable formation of a low-density tetrahedrally coordinated environment around water molecules. This leads eventually to an increase in entropy with density at constant temperature, which strongly influences the thermodynamics of water.
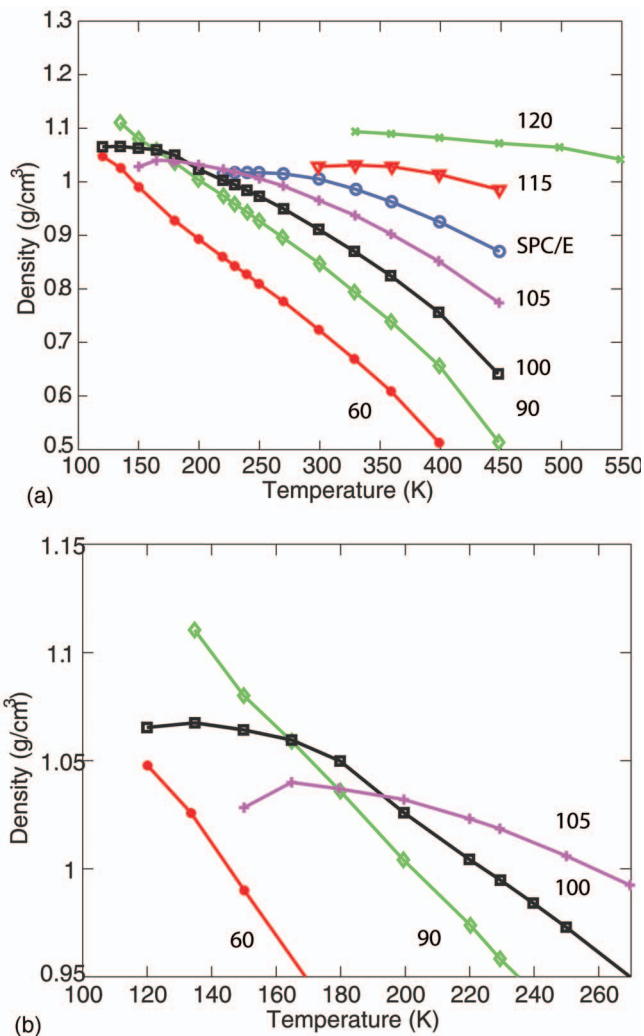

FIG. 2. (Color) (a) Equation of state of various bent models at a $P = 1$ bar. Each curve is labeled by the corresponding H–O–H angle. (b) Detail of the bent model equations of state at low temperature. The standard deviation of simulated density values is $0.001 - 0.005$ g/cm³.

Most well-known models of water, including SPC/E, exhibit the density anomaly.[10,25–28] The existence of this anomaly in the different bent models can be seen in Fig. 2. Like SPC/E water, B100, B105, and B115 exhibit density maxima in the liquid phase at 1 bar. B60 and B90 show no indication of a vanishing thermal expansion coefficient even at 120 K, the lowest temperature simulated in this work. B120, on the other hand, falls out of equilibrium below 330 K, but shows behavior consistent with approaching a state of vanishing thermal expansion.

The temperature of maximum density (TMD) of water-like models is the pressure-dependent temperature at which the coefficient of thermal expansion vanishes. As shown in Fig. 3, the TMD increases linearly with the H–O–H angle, or in other words, the density anomaly is enhanced upon increasing the H–O–H angle. In contrast, reducing the H–O–H angle brings the two hydrogen atoms closer to each other as well as to the central oxygen atom due to the rescaling of the O–H bond distance to conserve the dipole moment of SPC/E in all models. This diminishes the ability of the bent mol-
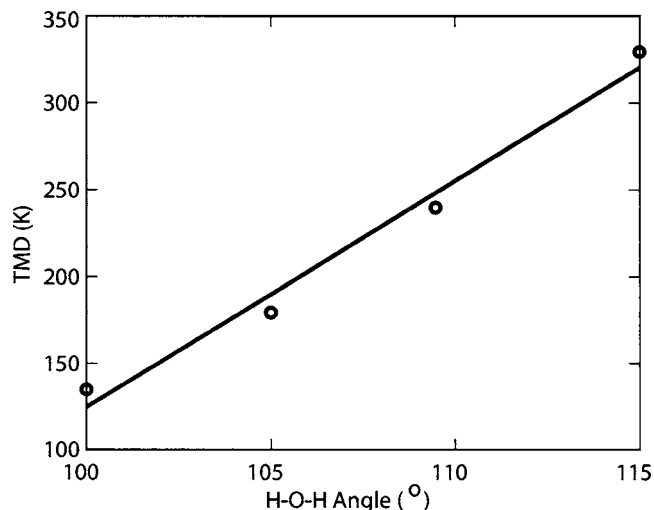
FIG. 3. Temperature of maximum density (TMD) at $P=1$ bar as a function of H–O–H angle for models exhibiting a density anomaly.

FIG. 5. MSD as a function of time at $T=250$ K and $P=1$ bar. Each curve is labeled with the corresponding H–O–H angle.

ecule to form an open hydrogen-bonded structure that is necessary for the occurrence of the density anomaly.

B. Dynamics

Figure 4 displays the mean squared displacement (MSD) as a function of time at 330 K. While B60, B90, B100, B105, and SPC/E show liquidlike diffusive behavior, B115 displays clear caging behavior before attaining the diffusive regime. For B120, caging persists throughout the entire simulation. The transition from the liquidlike diffusive behavior of SPC/E to the pronounced caging characteristic of supercooled liquid behavior as seen in B115 is abrupt, given that the difference in H–O–H angle is only 5°. As seen in Figs. 5 and 6, the onset of caging occurs at lower H–O–H angle upon cooling. The pronounced slowing down of diffusive motion with increasing H–O–H angle is related both to the associated increase in density [as seen in Fig. 2(a)] and to an increase in structural order, as will be discussed below.
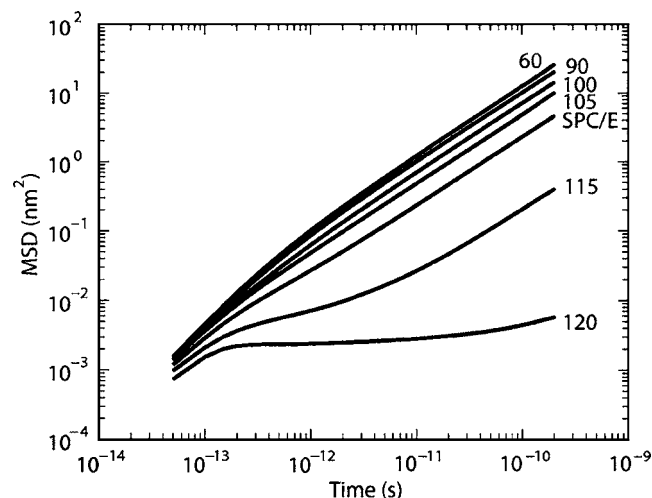
C. Structure

Spatial distribution functions for the different models were generated at three temperatures: 330, 250, and 200 K. The first-, second-, and third-neighbor shells are shown in Figs. 7 and 8 for $T=330$ K. A comparison of the first shells for the different models shows the gradual development of two regions of localization of molecules around the hydrogen atoms upon increasing the H–O–H angle [upper lobes in Figs. 7(d), 7(g), 7(j), 8(a), 8(d), and 8(g)]. The appearance of these hydrogen bond-acceptor "clouds" is clearly seen in the progression from B60 to B100. A hydrogen bond-donor lobe [lower region in Figs. 7(a), 7(d), 7(g), 7(j), and 8(a)], corresponding to molecules near the oxygen lone pair, splits into two separate regions when the H–O–H angle is increased beyond the SPC/E value of 109.47° [8(d) for B115 and 8(g) for B120]. The transition from a linear chainlike structure (as seen in B60) to a three-dimensional waterlike tetrahedral arrangement (SPC/E) is also observed for the second- and third-neighbor shells.

The structure of the first neighbor shell for B60, B90,

FIG. 4. Mean squared displacement (MSD) as a function of time at $T=330$ K and $P=1$ bar. Each curve is labeled with the corresponding H–O–H angle.
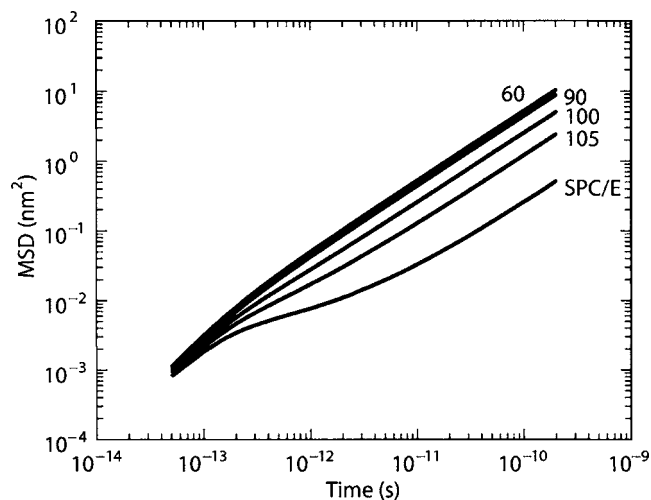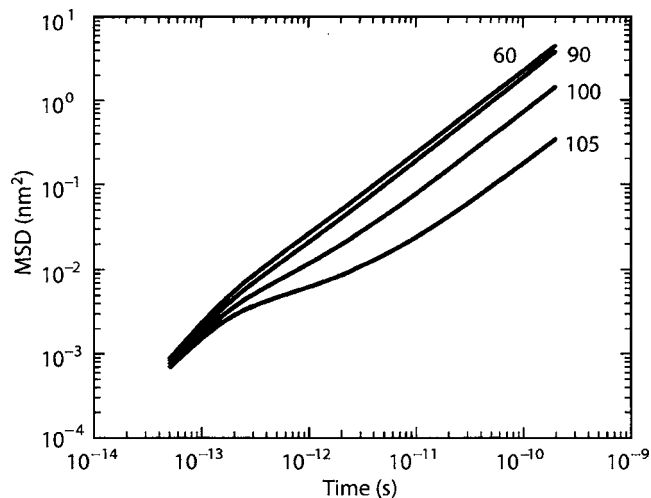
FIG. 6. MSD as a function of time at $T=200$ K and $P=1$ bar. Each curve is labeled with the corresponding H–O–H angle.
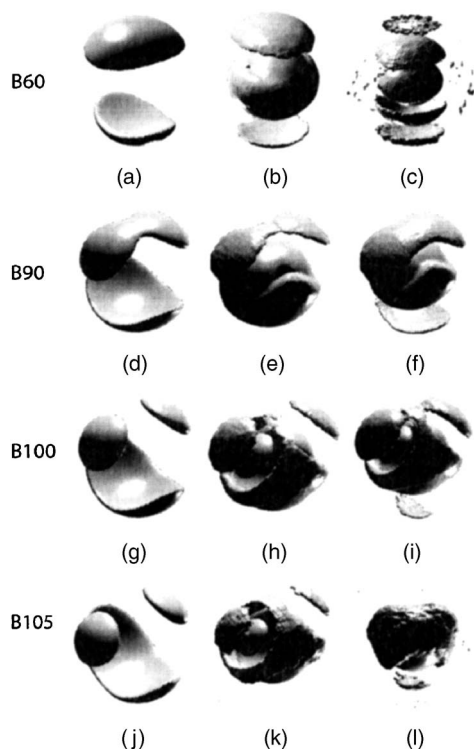
FIG. 7. Spatial distribution functions at $T=330$ K and $P=1$ bar showing the first three neighbor shells of bent models. [(a)–(c)] B60: Contour surfaces at {1.7, 1.3, 1.1} times the average water density; [(d)–(f)] B90: Contour surfaces at {1.7, 1.17, 1.1}; [(g)–(i)] B100: Contour surfaces at {1.7, 1.1, 1.05}; [(j)–(l)] B105: Contour surfaces at {1.7, 1.12, 1.05}.
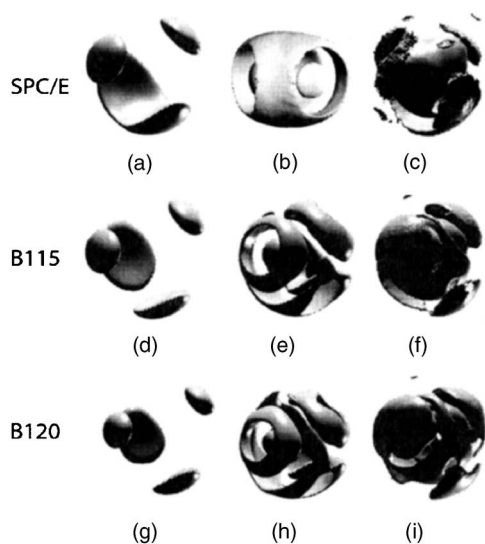

FIG. 8. Spatial distribution functions at $T=330$ K and $P=1$ bar showing the first three neighbor shells of bent models. [(a)–(c)] SPC/E: Contour surfaces at {1.7, 1.3, 1.1} times the average water density; [(d)–(f)] B115: Contour surfaces at {2.3, 1.4, 1.15}; [(g)–(i)] B120: Contour surfaces at {3.0, 1.4, 1.15}.
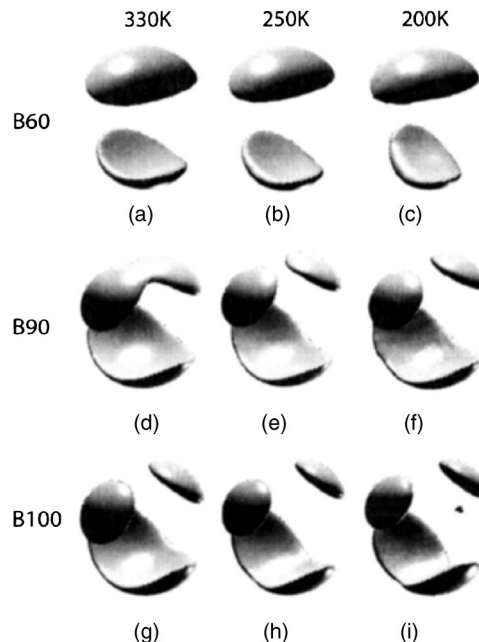

FIG. 9. Spatial distribution function at 1 bar showing the first three neighbor shells of bent models at 330, 250, and 200 K. [(a)–(c)] B60: Contour surfaces at {1.7, 1.6, 1.6} times the average water density; [(d)–(f)] B90: Contour surfaces at {1.7, 1.7, 2.0}; [(g)–(i)] B100: Contour surfaces at {1.7, 1.7, 2.0}.

and B100 at 330, 250, and 200 K is shown in Fig. 9. The first-neighbor shell for B60 is relatively unchanged over this temperature range. In contrast, both B90 and B100 gradually acquire waterlike structural features upon cooling. In the case of B100, this is manifested by the progressive narrowing of the hydrogen bond donor lobe and the widening of the distance between the hydrogen bond-receptor lobes. B90, in addition, develops a gradual split of the hydrogen bond-acceptor lobe.

A comparison of the oxygen-oxygen pair correlation functions for the different models at 330 K is shown in Fig. 10. The most striking observation from these plots is the shift of the second-neighbor peak from $r/\sigma_w=1.9$(B60) to $r/\sigma_w=1.63$(B120). This evolution entails a near-complete loss of structure beyond the first peak for intermediate H–O–H angles (e.g., B100, B105). It is important to note that this loss of structure beyond the first peak occurs in spite of the monotonic increase in density [$\rho=0.67$ g/cm^3 for B60 to $\rho=1.09$ g/cm^3 for B120; see also Fig. 2(a)] A useful way to represent the emergence of waterlike local order is to plot the ratio of the radial location of the second peak to that of the first peak as a function of the H–O–H angle. Figure 11 shows this ratio as a function of the H–O–H angle at 330, 250, and 200 K. At 330 K, we find that the bent models with H–O–H angles smaller than that of SPC/E have a peak location ratio of approximately 1.9, while for SPC/E, B115, and B120, the ratio is approximately 1.63. Both values of the ratio are significant because of their close correspondence with the LJ liquid value near the triple point[14] of approximately two and the experimental value for water[29] at 1 bar and 300 K, approximately 1.66. The angle associated with the transition between LJ-like and waterlike spherically averaged local structure decreases when the temperature is reduced, attaining a value of 100° at 250 K and 200 K. Thus, over the conditions investigated here, 100° appears to be the minimum H–O–H angle required to observe this waterlike structural characteristic.
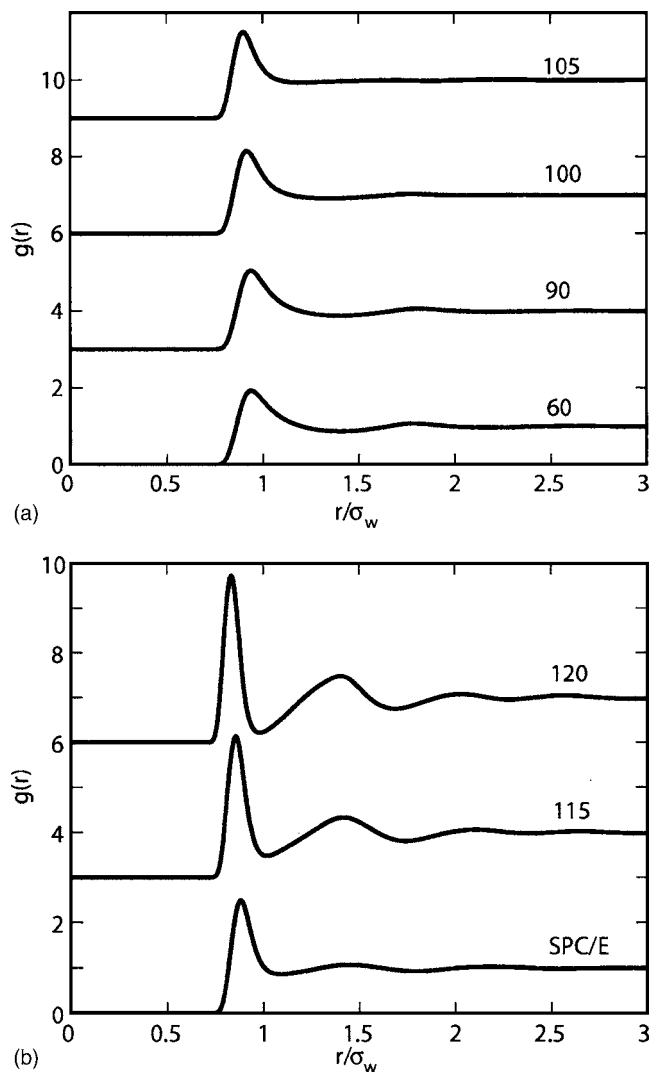
(a)

(b)

FIG. 10. Oxygen-oxygen pair correlation function for the various models at 330 K and 1 bar.

D. Order map

A useful way of quantifying structural order is to compute translational and orientational order parameters and to project the state of the system onto a plane whose coordinates are these order metrics. Such a representation, called the order map, was originally used to study the hard sphere system,[30] and has been subsequently applied to the Lennard-Jones system,[22] water,[23] silica,[31] and spherically symmetric systems that display waterlike anomalies.[32] Here, we use the translational and tetrahedral order parameters (τ, q) defined Eqs. (4) and (5). We follow the evolution of structural order during isochoric quenches of SPC/E and various bent models, starting from an equilibrated configuration at 400 K and 1 bar, and ending at 10 K, according to the quench protocol described in Sec. II. We also follow the evolution of structural order in the corresponding inherent structures, as explained in Sec. II. In both cases (isochoric quench and inherent structures), we use the order map representation to follow the evolution of structural order. Figure 12 shows the succession of τ-q curves for the various bent models. Each model's behavior is represented by a pair of curves: A solid quench-
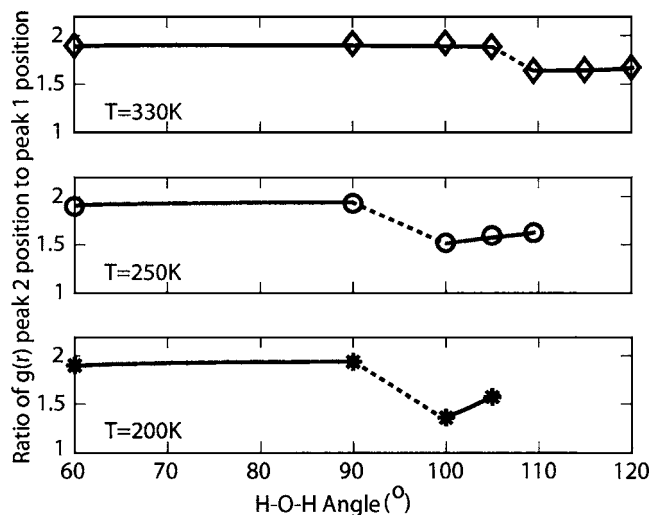

FIG. 11. Ratio of the radial location of the second peak of $g(r)$ to that of the first peak, as a function of the H–O–H angle at 330, 250, and 200 K. Pressure is 1 bar.

ing curve and a dashed inherent structure curve. Quenching the system to a sufficiently low temperature such as 10 K reduces thermal fluctuations so that the quenched configuration and inherent structure curves approach each other. Increasing the H–O–H angle appears to have the effect of increasing the tetrahedrality in the system. In every case except B60, the system evolves toward configurations of increased tetrahedrality upon cooling. In the case of B60, cooling causes a marked increase in τ, while q remains relatively unchanged, indicating the lack of tetrahedral structural order for this model. The progressive enhancement of tetrahedrality upon increasing the H–O–H angle is evident. Models with H–O–H angles $\geqslant 100°$ display qualitatively similar be-

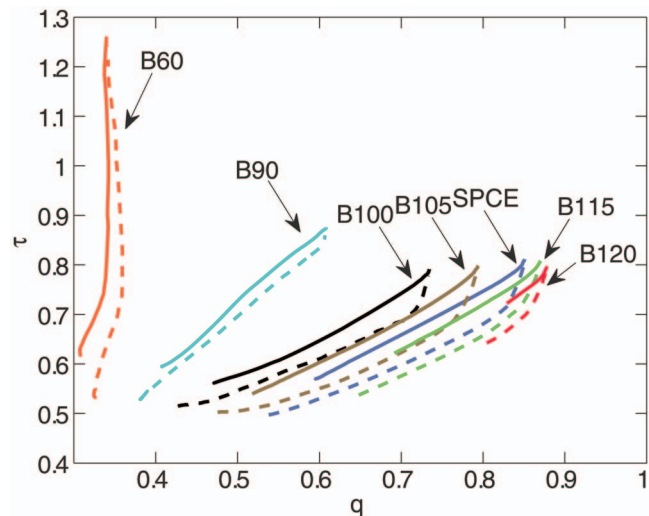
FIG. 12. (Color) Order map of translational (τ) vs orientational (q) metrics for the various bent models. The solid lines represent evolution of order metrics upon isochoric quenching from 400 to 10 K [density in each case corresponding to 1 bar at 400 K, see Fig. 2(a)], as described in the text. The dashed lines represent the corresponding inherent structures, generated as described in the text. For each pair of solid and dashed curves, temperature decreases as order parameters increase from bottom left to upper right. In the B60 case, temperature decreases in the direction of increasing translational order τ.
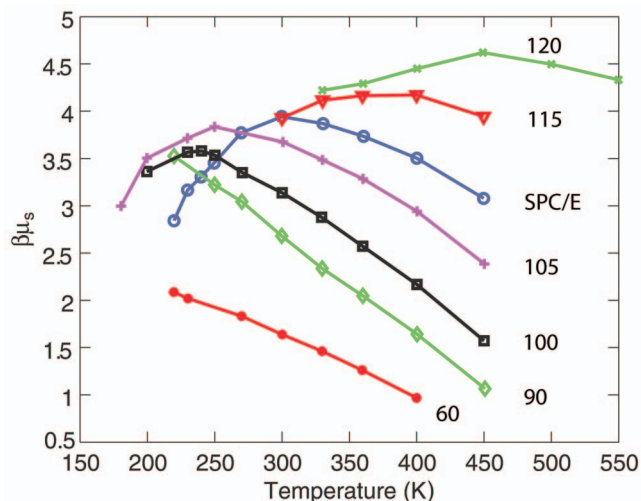
FIG. 13. (Color) Excess chemical potential at infinite dilution [multiplied by $\beta=1/(k_BT)$] as a function of temperature for a Lennard–Jones solute with $\sigma=3.16$ Å and $\epsilon=0.6502$ kJ/mol in the various water models at $P=1$ bar. The standard deviation is 0.1.

FIG. 14. Excess chemical potential at infinite dilution [multiplied by $\beta=1/(k_BT)$] as a function of temperature for a Lennard–Jones solute with $\sigma=6.00$ Å and $\epsilon=0.6502$ kJ/mol in the various water models at $P=1$ bar. The standard deviation is 0.1.

havior. Clearly, B90 can be viewed as an intermediate case between the linear and waterlike cases. It can be seen that increasing the H–O–H angle shortens the trajectory in the order map, dramatically so in the case of B120.

E. Solvation thermodynamics

The unusual properties of water extend beyond its behavior as a pure substance. A solute molecule, when placed in water, interacts with the hydrogen-bonded network of surrounding water molecules. Water's attempt to maintain the integrity of this network places orientational constraints on the hydration shell of the solute.[33] Competing enthalpic and entropic contributions influence the free energy of transferring a solute into water. The opposing nature and temperature dependence of these contributions leads to the nonmonotonic temperature dependence of the solubility of small apolar solutes in water, a distinguishing feature of hydrophobic hydration. At low temperatures, an unfavorable, negative dissolution entropy is compensated by a favorable, enthalpic contribution, while at higher temperatures, dissolution is entropically favorable and enthalpically unfavorable. This gives rise to a maximum in the solute's chemical potential and hence to a solubility minimum.

Here, we study the solvation properties of the different bent models using the Widom particle-insertion technique described in Sec. II. In separate sets of simulations, two LJ solutes, one with the same size parameter as SPC/E water, 3.16 Å, and another of size of 6 Å, were randomly and repeatedly inserted into systems of bent molecules at 1 bar and over a broad range of temperatures. The depth of the potential ϵ_s was set equal to that of water, 0.6502 kJ/mol. The excess solute chemical potential at infinite dilution relative to the ideal gas state was obtained from this calculation [see Eq. (2)]. Figures 13 and 14 show the variation of the solute's excess chemical potential with temperature in the various models. For a solute size of 3.16 Å (Fig. 13), we observe that all bent models with a H–O–H angle of at least 100° exhibit
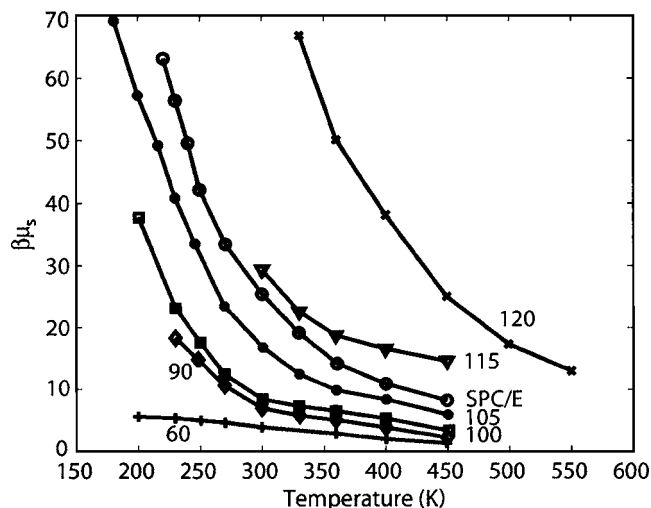
chemical potential maxima. This is a strong indication of a solubility minimum, although the latter is a property of a mixture with a finite solute mole fraction, whereas the chemical potential reported here is at infinite dilution. The temperature at which the chemical potential maximum occurs increases with the H–O–H angle. At $T \geqslant 300$ K, the solute's chemical potential increases with the H–O–H angle, indicating that the solvent becomes progressively more hydrophobic as the H–O–H angle is increased. Because the temperature at which the solute's chemical potential attains a maximum varies with the H–O–H angle, the relationship between solute chemical potential and H–O–H angle becomes nonmonotonic at low enough temperatures.

Upon increasing the solute size to 6 Å (Fig. 14), its chemical potential exhibits monotonically decreasing behavior with temperature. The monotonicity indicates that the anomalous increase in solubility with temperature observed for the smaller solute in B100, B105, SPC/E, B115, and B120 is suppressed by increasing the solute size. For this large apolar solute, there is a monotonic relationship between H–O–H angle and hydrophobicity at all temperatures. The solvation behavior of the larger 6 Å solute can be explained in terms of an increased enthalpic cost of creating a larger cavity in the solvent. The slope of each curve in Fig. 14 is equal to the ratio of the molar enthalpy of solvation to the square of the temperature. The observed decrease in the slope with temperature for the different bent models is therefore related to an increased ease of forming large cavities.

IV. CONCLUSIONS

In this work, we have studied the thermodynamics, translational dynamics, liquid structure, and solvation thermodynamics with respect to apolar solutes of a family of modified water models at atmospheric pressure and over a broad range of temperature ($130 \leqslant T \leqslant 550$ K). These bent models, which are perturbations of the SPC/E model, have H–O–H angles ranging from 60° to 120° (B60–B120), O–H

lengths ranging from 0.67 Å (60°) to 1.15 Å (120°), and the same Coulombic charges as the SPC/E model, thereby conserving the overall dipole moment of the SPC/E model. This study adds to a growing body of work[2–4] aimed at understanding the individual contributions of different aspects of water's molecular interactions to this substance's remarkable properties.

The geometric perturbations of the SPC/E model affect its waterlike thermodynamic properties. Decreasing the H–O–H angle leads to a shift of the density maximum anomaly to lower temperatures. We observe that an angle of at least 100° is required for observing a density maximum at atmospheric pressure with the TMD increasing linearly with H–O–H angle. The increase in the TMD indicates that the formation of a comparatively open hydrogen-bonded network, which is characteristic of waterlike behavior, persists up to progressively higher temperatures as the H–O–H angle is increased. Similar results are obtained for the solvation behavior of the bent models with respect to a small apolar solute. The solute's chemical potential exhibits a maximum with respect to temperature, which is also typical of waterlike behavior. This maximum is shifted to higher temperatures upon increasing the H–O–H angle. A minimum H–O–H angle of 100° is again required for waterlike behavior to be observed. Although we define waterlike thermodynamic anomalies in terms of the isobaric temperature dependence of the density or the solute's chemical potential, it should also be remembered that an important effect of increasing the H–O–H angle is to make the liquids denser [see Fig. 2(a)].

The combined effects of enhanced tetrahedrality and increased density cause a pronounced slowing down of translational mobility, and we observe glasslike loss of ergodicity below 330 K (B120) and 300 K (B115). The structural analysis reveals an evolution from a quasilinear local arrangement of neighboring molecules (B60) to a waterlike tetrahedral local environment (B100, B105, SPC/E, B115, and B120). Since elements of these two structures are incompatible, this evolution entails liquid structures which upon spherical averaging, exhibit virtually no pair correlation beyond the first neighbor shell (B100, B105).

By focusing on the individual contribution of the H–O–H angle on the structural, dynamic, and thermodynamic properties of a series of modified water models, we are able to determine that a minimum such angle of 100° is needed in order to support density anomalies and solubility extrema for small apolar solutes. Extending the present study to higher pressures, probing rotational dynamics, and calculating liquid-state order maps of this family of models are among the interesting investigations suggested by our study. We plan to pursue these in our future work.

[1] P. G. Debenedetti, J. Phys.: Condens. Matter **15**, R1669 (2003).
[2] D. L. Bergman and R. M. Lynden-Bell, Mol. Phys. **99**, 1011 (2001).
[3] R. M. Lynden-Bell and P. G. Debenedetti, J. Phys. Chem. B **109**, 6527 (2005).
[4] R. M. Lynden-Bell and T. Head-Gordon, Mol. Phys. **104**, 3593 (2006).
[5] P. E. Mason and J. W. Brady, J. Phys. Chem. B **111**, 5669 (2007).
[6] H. J. C. Berendsen, J. R. Grigera, and T. P. Straatsma, J. Phys. Chem. **91**, 6269 (1987).
[7] I. M. Svishchev and P. G. Kusalik, Chem. Phys. Lett. **215**, 596 (1993).
[8] I. M. Svishchev and P. G. Kusalik, J. Chem. Phys. **99**, 3049 (1993).
[9] J. L. Finney, A. Hallbrucker, I. Kohl, A. K. Soper, and D. T. Bowron, Phys. Rev. Lett. **88**, 225503 (2002).
[10] M. W. Mahoney and W. L. Jorgensen, J. Chem. Phys. **112**, 8910 (2000).
[11] J. L. F. Abascal and C. Vega, J. Phys. Chem. C **111**, 15811 (2007).
[12] J. L. F. Abascal and C. Vega, Phys. Chem. Chem. Phys. **9**, 2775 (2007).
[13] H. J. C. Berendsen, J. P. M. Postma, W. F. vanGunsteren, A. Dinola, and J. R. Haak, J. Chem. Phys. **81**, 3684 (1984).
[14] M. P. Allen and D. J. Tildesley, *Computer Simulation of Liquids* (Clarendon, New York/Oxford University Press, Oxford, 1987).
[15] J. P. Ryckaert, G. Ciccotti, and H. J. C. Berendsen, J. Comput. Phys. **23**, 327 (1977).
[16] B. Widom, J. Chem. Phys. **39**, 2808 (1963).
[17] F. H. Stillinger and T. A. Weber, Phys. Rev. A **25**, 978 (1982).
[18] N. Giovambattista, P. G. Debenedetti, F. Sciortino, and H. E. Stanley, Phys. Rev. E **71**, 061505 (2005).
[19] L. D. Landau and E. M. Lifschitz, *Mechanics*, 3rd ed. (Pergamon, Oxford, 1976).
[20] S. Torquato, T. M. Truskett, and P. G. Debenedetti, Phys. Rev. Lett. **84**, 2064 (2000).
[21] T. M. Truskett, S. Torquato, and P. G. Debenedetti, Phys. Rev. E **62**, 993 (2000).
[22] J. R. Errington, P. G. Debenedetti, and S. Torquato, J. Chem. Phys. **118**, 2256 (2003).
[23] J. R. Errington and P. G. Debenedetti, Nature (London) **409**, 318 (2001).
[24] P. L. Chau and A. J. Hardwick, Mol. Phys. **93**, 511 (1998).
[25] L. A. Baez and P. Clancy, J. Chem. Phys. **101**, 9837 (1994).
[26] I. M. Svishchev, P. G. Kusalik, J. Wang, and R. J. Boyd, J. Chem. Phys. **105**, 4742 (1996).
[27] M. L. Tan, J. T. Fischer, A. Chandra, B. R. Brooks, and T. Ichiye, Chem. Phys. Lett. **376**, 646 (2003).
[28] C. Vega and J. L. F. Abascal, J. Chem. Phys. **123**, 144504 (2005).
[29] A. Rahman and F. H. Stillinger, J. Chem. Phys. **55**, 3336 (1971).
[30] S. Torquato, T. M. Truskett, and P. G. Debenedetti, Phys. Rev. Lett. **84**, 2064 (2000).
[31] M. S. Shell, P. G. Debenedetti, and A. Z. Panagiotopoulos, Phys. Rev. E **66**, 011202 (2002).
[32] Z. Y. Yan, S. V. Buldyrev, N. Giovambattista, and H. E. Stanley, Phys. Rev. Lett. **95**, 130604 (2005).
[33] H. S. Ashbaugh, T. M. Truskett, and P. G. Debenedetti, J. Chem. Phys. **116**, 2907 (2002).